Composites: Part B 56 (2014) 821–829

Contents lists available at ScienceDirect

Composites: Part B

journal homepage: www.elsevier.com/locate/compositesb

Damage characterization of surface and sub-surface defects in stitch-bonded biaxial carbon/epoxy composites

Masoud Yekani Fard [a,*], Seid Mohammadali Sadat [a], Brian B. Raji [b], Aditi Chattopadhyay [a]

[a] School for Engineering of Matter, Transport and Energy, Arizona State University, AZ 85287, USA
[b] Pipe Reconstruction Inc, 2800 North Central Avenue, Phoenix, AZ 85004, USA

ARTICLE INFO

Article history:
Received 1 October 2012
Received in revised form 3 September 2013
Accepted 7 September 2013
Available online 20 September 2013

Keywords:
A. Polymer–matrix composites
B. Defects
C. Damage mechanics
D. Mechanical testing

ABSTRACT

The scope of this work is to study the effects of manufacturing and installation defects on mechanical performance of polymer matrix composites appearing in civil infrastructure and aerospace applications. The objective of this study is to create a link between defects detected through nondestructive testing (NDT) and the mechanical performance of the composite structures using strain mapping technique. Monotonic tensile samples of polymer matrix stitch-bonded biaxial composite laminates [90,0]s are tested. Flash Thermography, a conventional NDT technique, is used to predict detectable pre-existing surface and sub-surface irregularities and defects. Attention is drawn to the homogenized mechanical behavior and to damage initiation and propagation. Damage onset and propagation are studied using time-dependent nonlinear regression of the strain field. Effects of the manufacturing and installation irregularities on damage initiation, propagation, and failure are monitored as the structure is subjected to load or studied at the end of the loading process.

1. Introduction

The use of composite materials is driven by the need for strong and lightweight structures, which is why applications of different composite materials in the aerospace and civil infrastructure industries, such as power plants, have taken on ever-increasing importance. Additionally, one of the most important challenges of today is the repair of deteriorated and damaged infrastructures – such as buried steel and concrete pipes that have been in service for more than several decades. Composite materials have many advantages over other structural materials, mainly due to their high specific strength and specific stiffness; however, their general application has suffered from difficulties associated with installation and inspection of hard-to-access structures (Fig. 1) [1]. Improvement of mechanical properties, particularly interlaminar shear of stitch-bonded composites in comparison with un-stitched, has been confirmed in the literature [2–4]. However, the prediction of mechanical performance of stitched laminates under real operational conditions is very complicated. Understanding actual failure mechanisms begins with identification of the weakening areas (or load concentration areas) such as a hole, notch, cutout, bolted joint, and a manufacturing defect (a fiber ends or a free edge) [5]. Irregularities in composites due to manufacturing and installation-induced scenarios are generally related to the curing procedure of composite materials, in addition to the extreme environmental conditions (e.g., temperature and moisture) that can occur during the fabrication and installation processes. When composite parts are transported from the factory to the industrial site, they may be accidentally exposed to moisture. Humidity can also lead to a loss of performance in polymer matrix composite materials. Irregularities, such as deviation of strands from their theoretical position can occur in dry fiber strands or during the injection/installation process. While irregularities on the surface of composite samples can be detected by the naked eye, the degree to which manufacturing and installation-induced defects influence the mechanical performance of composites is still not fully understood, and therefore represents a challenge, especially in the context of repairing and maintaining aerospace and civil industry applications.

The mechanical properties of laboratory-cured composites and the formation of damage and its influence on composite properties have been studied extensively [3–12]. Vallons et al. [7] used X-ray radiography to monitor damage evolution at certain cycles in fatigue tests. Lomov et al. [6] and Giordano et al. [9] used acoustic emission, X-ray, and ultrasonic C-scan to study damage in laboratory-cured composite samples. Some of these NDE techniques such as ultrasonic C-scan and X-ray are not on-line based techniques and require the targeted structural component to be taken out for a period of time for damage inspection and assessment [10]. On-line health monitoring techniques such as piezoelectric sensor and optical fiber involve the attachment of an external sensor or

* Corresponding author. Tel.: +1 480 370 9786.
E-mail address: Masoud.yekanifard@asu.edu (M. Yekani Fard).

1359-8368/$ - see front matter © 2013 Elsevier Ltd. All rights reserved.
http://dx.doi.org/10.1016/j.compositesb.2013.09.011

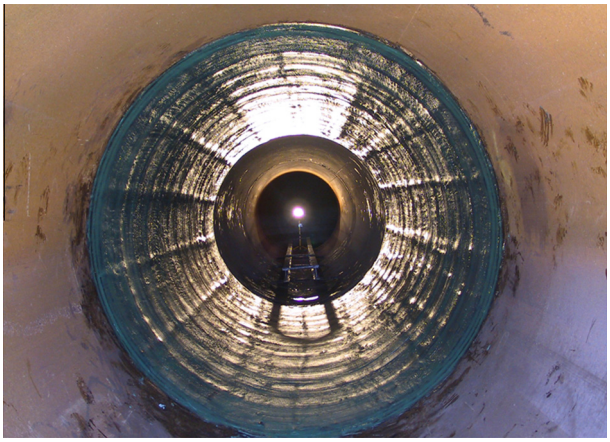

Fig. 1. Carbon fiber composite repair of 3m pipe underground.

additional fibers in composite structures [11,12]. Most of the embedded or attached sensors are not durable and are difficult to repair. DC and AC electrical conduction measurements have been used for detection of damage in composites for fiber failure and matrix cracking, delamination, and fiber/matrix debonding, respectively [13]. However, detection of damage locations and sizes from electrical resistance changes is not always a straight forward process. Statistical tools and inverse problem algorithms are necessary to locate delamination [14]. Markatos et al. [8] investigated the effects of different manufacturing-induced and in-service defects on the mechanical performance of composite structures.

Laser Raman spectroscopy has been widely used to non-destructively measure strain and stress fields and to investigate the macro-mechanical performance of a damaged specimen [15–19]. Potluri et al. used this method to measure in situ fiber strains [19]. In this method, the strain values are obtained from the embedded reinforcing bars. Some amorphous fibers such as glass fibers have a very weak Raman response and cannot be used for strain measurements [20]. Katerelos et al. [20] studied residual strain and modulus reduction due to cracking in cross-ply GFRP composites using Kevlar fibers as Raman strain sensors. Moire Interferometry [21–23] and grating shearography [24] have also been employed to investigate surface strain field in textile composites. The effects of pre-existing defects on surface strain distributions were ignored in these studies.

Image correlation has been used to perform an extensive study of surface strain fields and for characterization of nonlinear material behavior [25–32]. The DIC system is a powerful optical measurement tool with sufficient accuracy for strain measurements and understanding of micromechanical behavior of composite systems [33–35]. For example, Godara and Raabe [33] studied the influence of fiber orientation on global mechanical behavior and strain localization in glass fiber reinforced polymer composites during tensile tests. Gao et al. [35] analyzed damage evolution in Kevlar composites using the DIC technique. However, DIC measurements are also accompanied by noise. Linear regression was used by Lomov et al. [28] to determine just the damage initiation for the linear elastic behavior. Lee et al. [24] employed a Gaussian low-pass filtering method to remove noise. In modern thermography practices, Flash Thermography has been routinely used to measure plate thickness and thermal diffusivity [36–38]. The cases discussed in the cited research represent a range of idealized conditions where the samples used were laterally infinite with no edge or boundary condition effects. A missing element in the current literature, however, is the examination of the effects of pre-existing defects and "irregularities" on the mechanical behavior of anisotropic composite materials.

Descriptions of composite laminates are based on simplifying assumptions related to the geometrical periodicity of strands. However, in reality, the geometrical periodicity is not fully maintained due to stochastic variations of the strand dimensions and placements. Development of different damage modes in relation to the internal structure of non-crimp fabric reinforced composites was studied by Greve and Pickett [39] and Mattsson et al. [3]. They observed cracks in fiber bundles at the onset of damage followed by local delamination which lead to premature fiber damage. Random placement of the laminas in a composite laminate in the form of *nesting the layers* may not affect the homogenized mechanical properties of the laminate, but it can lead to resin-rich zones and influence the strain fields. Also, actual fiber volume fractions may vary across the composite laminate, especially under not fully controllable conditions during fabrication and installation at industrial sites. Some of these variations or "irregularities" may be identified by NDT and structural health monitoring techniques.

Due to the high biaxial performance of stitch-bonded composites, these fabrics are highly desirable materials for pipe coatings and for the rehabilitation of civil infrastructures. In this paper, damage characterization in stitch-bonded carbon/epoxy biaxial composites – initiation and development will be studied. Damage at the macro level involves stiffness reduction, maximum strength, and failure strain. Meso-level damage is related to damage initiation sites inside the structure of the reinforcement (strands) and associated deterioration of the homogenized mechanical properties of the composites. Meso-level in bidirectional composite defines the internal structure of the reinforcement and the variation in fiber volume fraction. The study is focused on issues that have not been sufficiently addressed in the current literature.

The present work also aims to contribute to the understanding of the relationship between NDT and in situ monitoring techniques through an analysis of surface and subsurface damage that can compromise the quality of composite structures as a function of loading. The following areas are investigated: (1) Tensile tests on samples cut from plates fabricated in the industrial site accompanied with optical-extensometer are performed to produce stress strain curves and to identify strain levels characteristic of: (i) first damage visible at the macro-scale; (ii) developed damage; and (iii) failure strain before final fracture. (2) Flash Thermography tests are used to reveal pre-existing damage induced by the manufacturing and installation processes. (3) A full-field strain mapping technique is employed to highlight the relationship between strain concentrations linked with the surface and subsurface irregularities associated with damage initiation and development. The effectiveness of nonlinear-regression time-wise filtering to remove noise from the signals is investigated. (4) Damage propagation and associated

Table 1
Specifications of the resin and fiber.

Resin PRI 2002-3-R-A	
Viscosity, cPs	3000
Glass transition temperature, °C	75
Specific gravity	1.16
Bulk density, pounds/gallon	9.74
Ingredients:	Concentration
Bisphenol-A type epoxy resin	>50%
Bisphenol-F type epoxy resin	<40%
Aliphatic glycidyl ether	<20%
Continuous filament carbon fiber PRI 2000-1-C bounded by polyester stitching	
Carbon fiber tow	~94 wt.%
Sizing	~4 wt.%
Texturized polyester yarn	~2 wt.%
Specific gravity	1.6–2.0

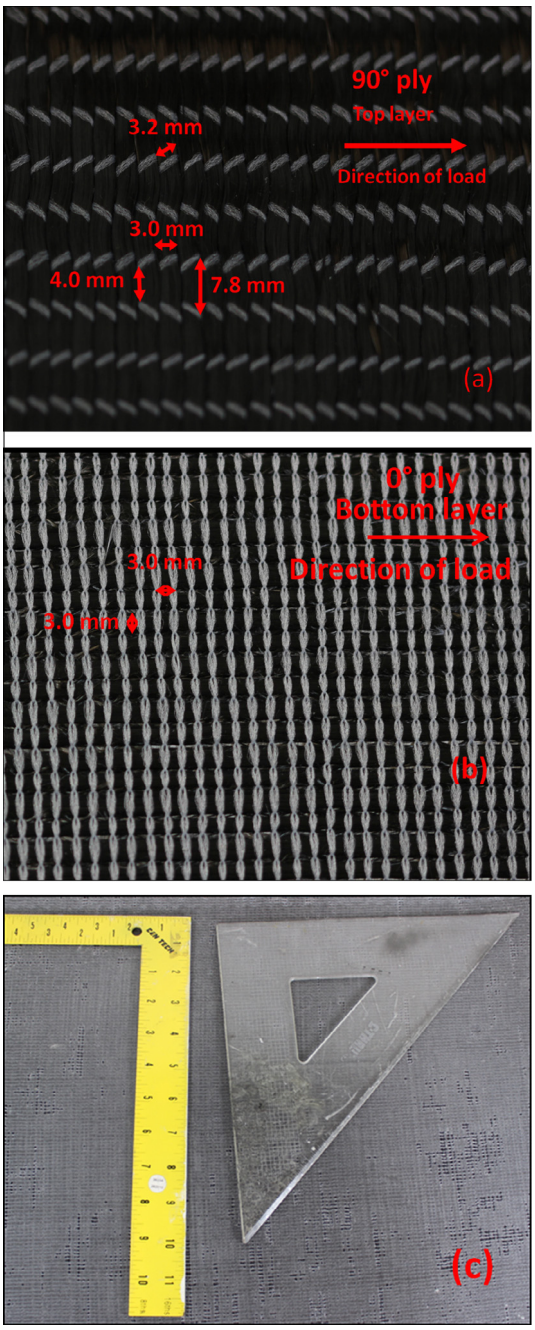

Fig. 2. Biaxial dry fiber reinforcement: (a) top layer 90°; (b) bottom layer 0°; (c) misalignment of fibers in a composite plate fabricated in industrial site.

reduction of composite stiffness are analyzed. (5) An adaptive algorithm for online damage detection to indicate the influence of the pre-existing irregularities on damage propagation and failure is examined.

2. Material and specimens

Stitch-bonded continuous filament carbon fibers (biaxial fabric PRI 2000-1-C) and resin (PRI 2002-3-R-A) with catalyst (PRI 2000-5-HR-B) provided by Pipe Reconstruction Inc. were used in this study. The specifications of the fiber and the resin are listed in Table 1. Two biaxial fabric laminas, as shown in Fig. 2, were used to fabricate a composite plate with the stacking sequence of [90/0]s giving an average thickness of 4.6 ± 0.04 mm and an average

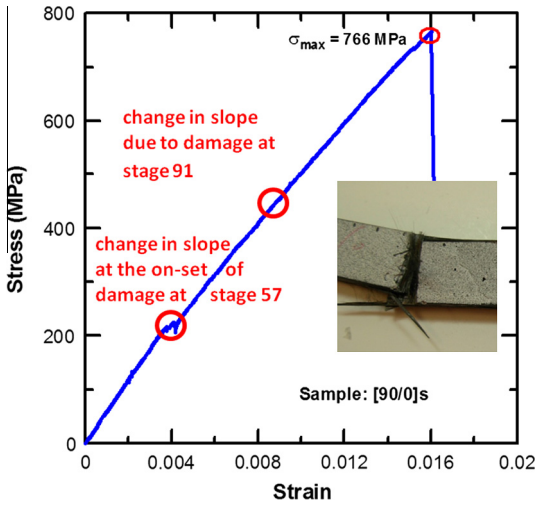

Fig. 3. Tensile stress–strain diagram for [90/0]s composite laminate; points correspond to slope changes in the diagram.

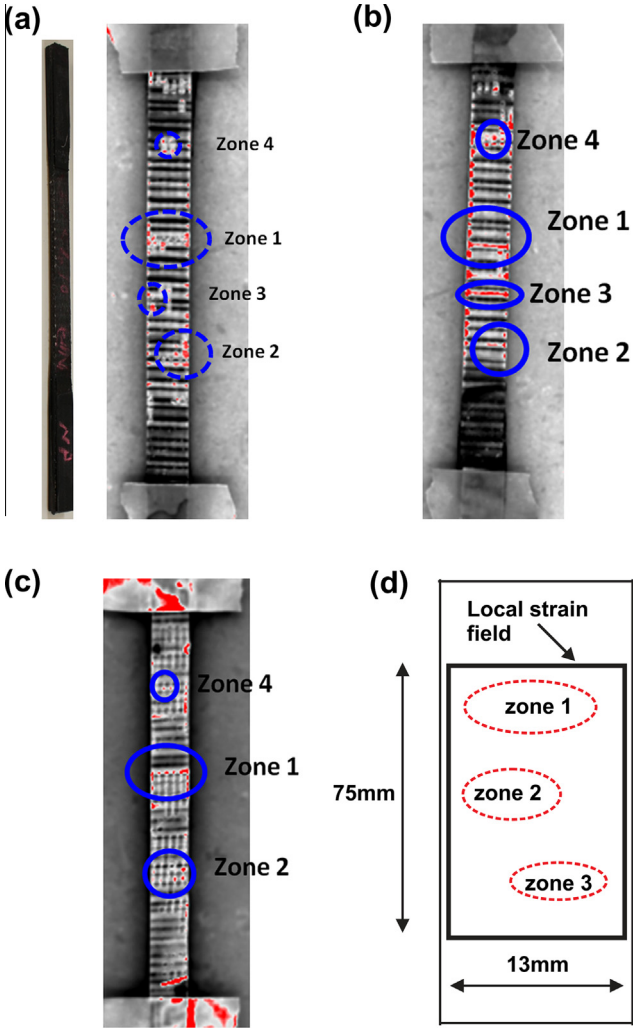

Fig. 4. (a)–(c) Irregularities and surface/subsurface pre-existing defects in samples one, two, and three; (d) field of view for local strain field.

fiber volume fraction of 49 ± 1%. All samples have a nominal size of 310 mm length, 13.5 mm width and were cut from the plates using a water-cooled diamond saw. Composite end tabs were

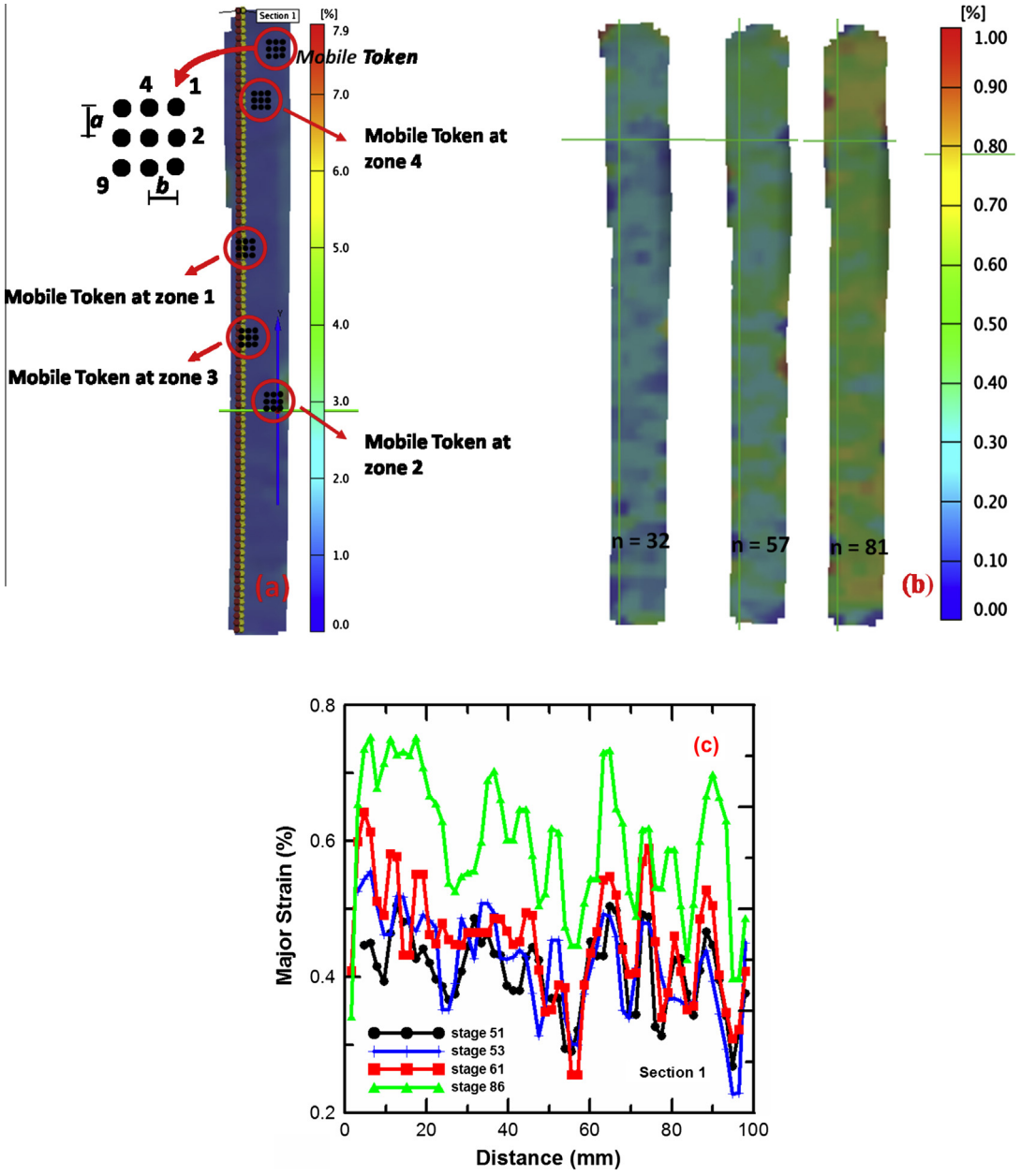

Fig. 5. (a) Major strain distribution and the location of mobile token at different zones (*a* and *b* are fractions of the unit cell); (b) vertical strain field at stages 32, 57, and 81; and (c) measured major strain profile at different stages of loading.

constructed from the same material, but cured under laboratory conditions and attached onto the samples using the same resin.

3. Mechanical tests

The tensile test, a common mechanical characterization test, simulates a plane stress strain state in the sample during the loading process. In this study, monotonic tensile tests were conducted according to ASTM 3039 [40]. Specimens of longer length than the minimum requirements of the standard were used to keep the field of view area as far from the grips as possible and as a way to obtain consistent results. The distance between the grips was 210 mm prior to introducing the load and the length of the tabs was approximately 90 mm. Tensile load was applied to the specimens under a constant strain rate of 22 μstr/s.

The samples were tested using an MTS biaxial/torsion test frame (50 KN capacity for each axis). Laser and grip alignment fixtures were used to mount the samples in the grips and to eliminate bending and premature failure. Appropriate grip pressure was used to avoid slippage and any premature failure of the specimen in the grip area. The DIC system, extensively used to study strain field and stress state and to develop constitutive stress–strain relationships [25–27], was used to perform the strain mapping study, and to determine the strain field and occurrence of cracks and failure. GOM ARAMIS 5M and 2M 3D with 5 and 2 mega pixels systems, respectively, were used in this study. Images were taken at a rate of 0.33 fps to obtain global strain. Local strain values were obtained over the area of interest (a rectangle surrounding the surface/subsurface defect zones) to study the strain field. The DIC system was used as an optical extensometer with no side or grip effects with a strain accuracy up to 100 μstr (Fig. 3). To ensure the software

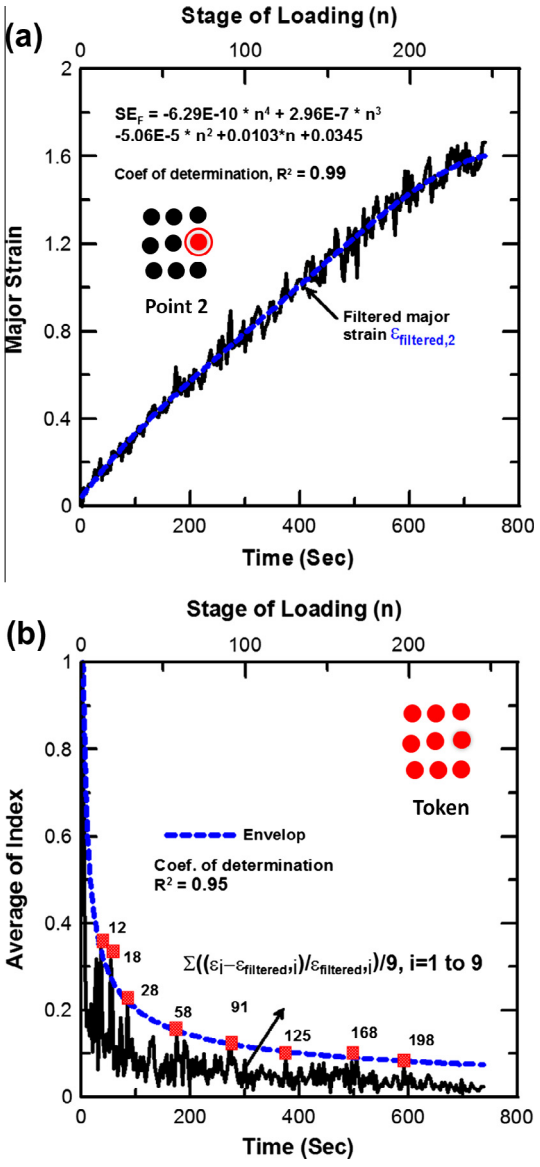

Fig. 6. (a) Registered major strain before filtering and filtered major strain after application of time regression at point 2 of the mobile token at zone 1, (b) envelope of the averaged index (relative noise level) of all points in the token in zone 1.

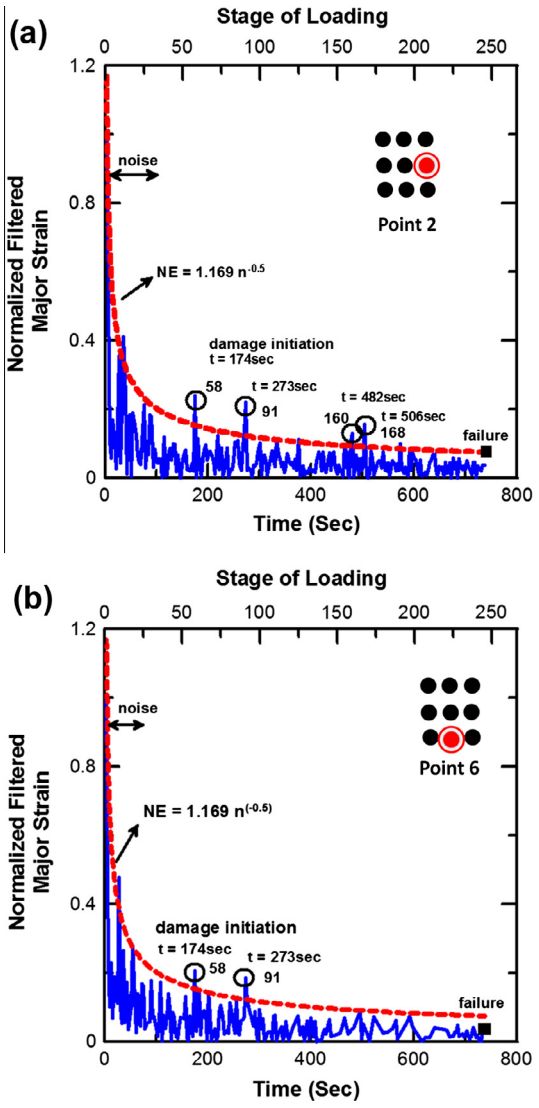

Fig. 7. Damage identification and development at the location of the pre-existing defect zone1.

achieves better image recognition, a random speckle pattern was applied to the surface of the samples. The facet size was 25×25 pixels with a 3×3 matching mode. Strain values in Fig. 3 are averaged strains calculated from full field strain measurements in the longitudinal direction. The points marked on the curve correspond to the strain levels where the non-linearity of the material response begins. A small stress drop typically referred to as "pop-ins" was observed at stage 57. After the load drop, stress increased with a reduced stiffness (a kink point at stage 91) until final fracture at 1.6% strain.

4. Results and discussion

4.1. Detection of pre-existing damage and irregularities

A Flash Thermography test is a sequence of a collection of pixel time histories obtained after flash heating the surface of materials [41]. As heat from the front travels toward the interior of the plate, subsequent cooling of the surface takes place. In thermographic analysis of the images, regions of contrast between discrete features and intact background areas can be visually identified and recognized as possible damaged areas.

In this study, experiments were conducted using a commercial pulsed-thermography system (EchoTherm, Thermal Wave Imaging, Inc.) with a 320×256 InSb IR focal plane array camera operating at 60 Hz. A composite plate with dimensions of 70 mm $\times$ 140 mm with several discrete flat bottom holes was used for the calibration. The flat bottom holes, ranging in diameter from 1 mm to 5 mm and in depth from 0.2 mm to 2 mm, were machined into the back side of the calibration plate. The regions of irregularities and possible surface/subsurface defects (seen in red color) in three samples were marked by a blue dashed circle as shown in Fig. 4(a–c). An analysis of the log temperature vs. the depth plot for a typical surface point shows that the deepest detectable defect is almost one third of the composite laminate thickness. Due to amount of energy input, only two thirds of the sample volume could be interrogated. Based on the Flash Thermography results, it was concluded that irregularities and pre-existing defects were present on the composite sample surface and subsurface; however, the effect on stress strain response was unknown. All three samples showed defects in zones 1, 2, 3, and 4 except sample in

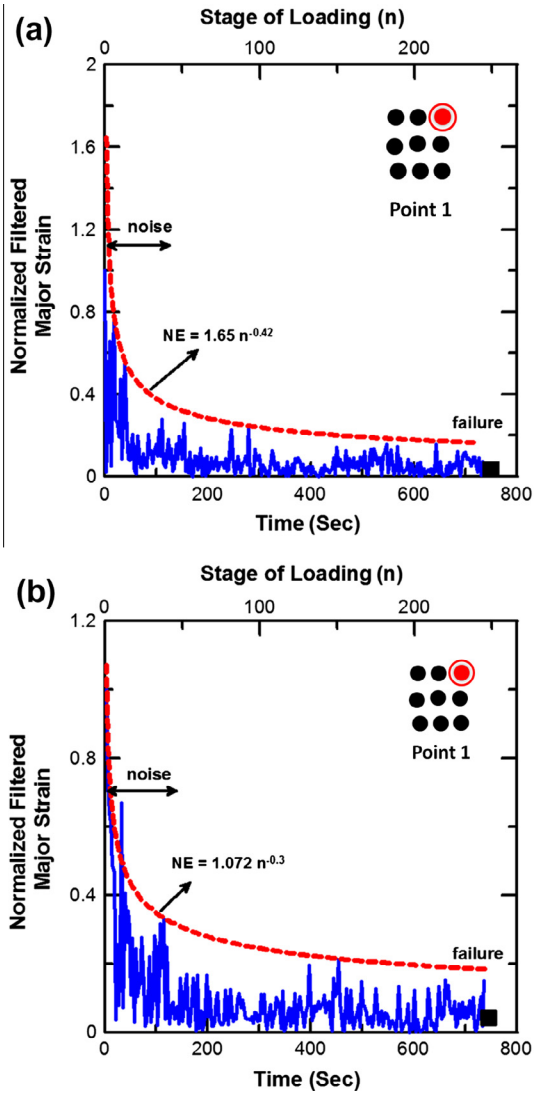

Fig. 8. No detectable damage identified in zone 2 (a) and 3 (b).

Fig. 4c which does not show any defect in zone 3. Fig. 4(d) shows the field of view for local strain field study.

4.2. Detection of damage initiation/propagation

Strain mapping is a system of determining strain fields using digital images taken while samples are loaded. As tensile load is applied, the system takes consecutive images and analyzes them, while comparing them to initial images in order to determine local displacement and engineering strain values. The following damage development scenarios are possible in stitch-bonded biaxial [90/0] composite laminates: (i) onset of cracks (matrix or inter-fiber or intra-strand) in a 90° layer; (ii) onset of local delamination on the boundaries of fiber strands (ends); (iii) onset of fiber failure, large delamination zones, and ultimate failure of the samples. The definition of "damage initiation" can be fairly fuzzy since the source of cracks due to different pre-existing irregularities and defects is unknown; in this context, we consider the damage initiation strain to be an indication of a crack (coalesced cracks) associated with the transition from the initial linear behavior of the stress–strain curve to its nonlinear behavior. At the damage initiation stage, very few cracks will be present, and most likely these will appear at the location of pre-existing defects. Further accumulation of damage, however, may lead to several cracks distributed across the specimen (e.g., at the location of stress concentrations and not necessarily other identified pre-existing defects). The focus of this section is on damage initiation and propagation at the location of pre-existing defects.

Full-field strain mapping was registered using ARAMIS system in 3D mode. Fig. 5(a–c) presents full field DIC results for stages 51, 61, and 86 in the stress strain curve shown in Fig. 3. Fig. 5(d) shows the major strain distribution at different stages of the loading process along Section 1, which show the development of the same "hills and valleys" as observed in other studies [19,28]. The reason for the hills and valleys may lie in a non-ideal placement (misalignment) of fiber strands as evident in Fig. 2(c). This possibly happened during fabrication of the composite laminate in the industrial site because of relative flexibility of the structure of the fiber reinforcement. By choosing a higher strain field size than of 3×3 (e.g., 9×9), the sharpness of the hills and valleys can be smoothened. However, high strain field sizes will also wash out the local effects in the strain field.

The noise of the strain field was analyzed to evaluate the health condition in the irregular zones detected by Flash Thermography. The zone studied had the length of 75 mm (surrounding the defect zones) and covered the entire width of the specimen. The facet grid used is of a rectangular pattern with each facet incorporating (11×11) pixels. The strains at the early stages of loading were comparable with the noise level of the strain mapping. A mobile token 3×3 points, as shown in Fig. 5(a), was introduced to analyze the registered strain mapping. Time-dependent nonlinear regression was applied to every point of the mobile token in the registered major strain field to obtain the filtered major strain at that specific point, as shown in Fig. 6(a). At every point of the mobile token, a filtered strain tensor $SE_F = F(\boldsymbol{n}$ or $\boldsymbol{t}$ or $\varepsilon_{\boldsymbol{applied}})$ was introduced where the dependency is defined in terms of stage of loading $\boldsymbol{n}$, time $\boldsymbol{t}$, or the global applied strain $\varepsilon_{\boldsymbol{applied}}$.

For major strain components, a fourth order polynomial was considered. The relative noise level at every point i of the token and at any instant of time is calculated as $(\varepsilon_i - \varepsilon_{filtered,i})/\varepsilon_{filtered,i}$. The same filtering and time-dependent regression procedure can be applied to all the points of a mobile token to identify damage. The envelope function *NE* of the averaged relative noise levels of the token is considered as a threshold for the identification of damage (Fig. 6(b)). Points 2 and 6 (Fig. 7) clearly show damage initiation and development at the location of the pre-existing defect. The damage index *DI*, defined based on the ratio of the relative noise level to the envelope function, stays inside the limit for some stages of loading.

$$DI = \frac{(\varepsilon - \varepsilon_{filtered})/\varepsilon_{filtered}}{NE} \tag{1}$$

The reason for inconsistent damage identification throughout the loading phase may lie in the inhomogeneous nature of the composite material (due to pre-existing defects and irregularities) and redistribution of load among strands. The relative noise level is high at the early stages of linear elastic behavior due to the reason discussed earlier in this section and decreases as the local major strain increases. The definition of the damage index, as outlined in Eq. (1), considers the effects of nesting on strain fields. The same damage identification procedure was applied to zones 2 and 3, and no damage was detected through strain mapping, as evident in Fig. 8. Strain field data were not available in zone 4 of sample 1 due to the peeled-off surface in that area.

The few red marks observed in zones 2 and 3 (Fig. 5), from Flash Thermography, can be attributed to side effects or to pre-existing subsurface defects that do not influence strain field at the surface of the sample.

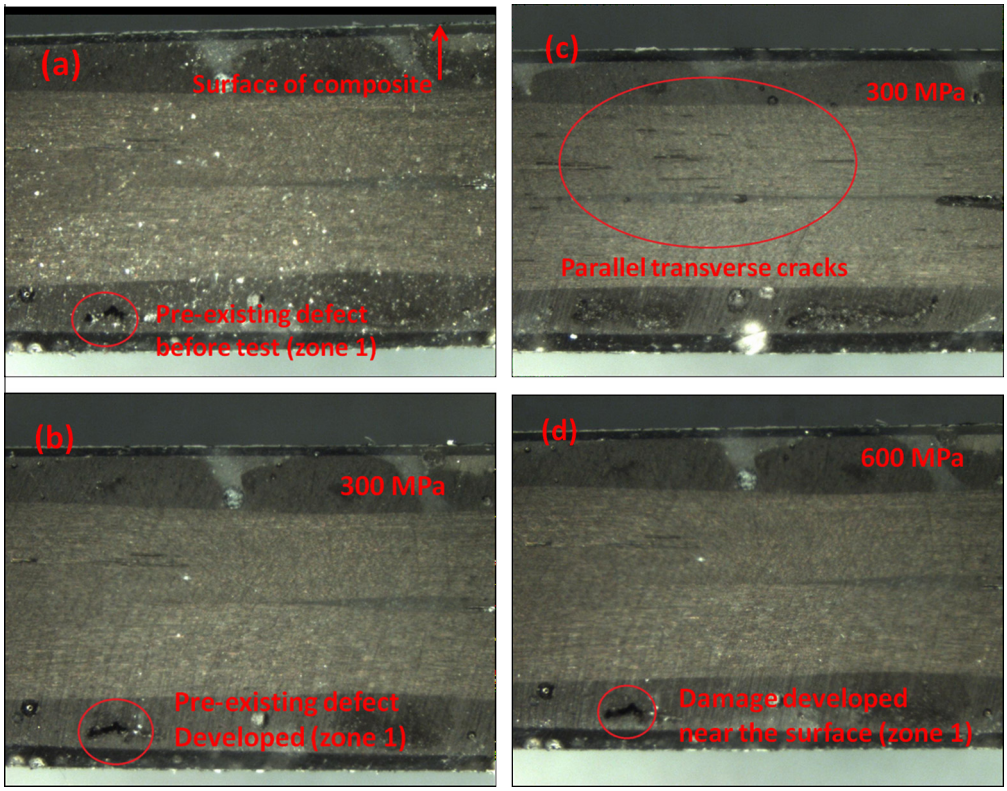

Fig. 9. Pre-existing cracks and damage in composite laminate [90/0]s. (a) pre-existing defect before test (sample one); (b) defect at zone 1 developed at 300 MPa (sample two); (c) parallel cracks formed in other parts of sample (sample three); (d) large damage at 600 MPa (sample two).

The damage state of the samples identified using optical microscopy reinforced the damage evolution results shown in Figs. 3, 7 and 8. Optical microscopy has been used to investigate the relationship between the development of damage and the change in stiffness in 2D and 3D woven composites [42–45]. Daggumati et al. [42] used optical microscopy to study damage initiation and propagation in weft yarns in a 5-harness satin weave carbon polyphenylene sulfide. Masters and Ifju [16] used optical microscopy post-mortem examination and X-ray to study damage development in 3D braided composites. Samples 2 and 3 were observed under 50× magnification. In the damage characterization process of healthy (with no pre-existing defects) composite samples, the following stages of damage development are expected [3,16,39,43–45]: (i) inter fiber and transverse cracks; (ii) delamination on the boundaries of the fiber bundles; and (iii) fiber failure and large size delamination. However, damage initiation/propagation may not follow the above classifications if there is a pre-existing defect in a composite sample. In addition to Flash Thermography, optical microscopy examination of the samples before the tensile test showed pre-existing defects near the surface at 90° lamina in zone 1 (Fig. 9(a)). It should be noted that only the most reliable trends of damage evolution, particularly in zones 1–4, were sought in this analysis. Furthermore, no effort was made in this study to directly associate a particular damage mode with stress drops and kink points. The optical microscopy results presented herein are however examined in comparison to damage states at stages 57 and 91 described before. The optical examination identifies the local damage modes. The pre-existing defect in zone 1 developed at 300 MPa load level, as shown in Fig. 9(b). Small cracks, perpendicular to the loading direction, had formed in the middle 0° layer in other parts of the sample. These cracks were parallel to the sample surface (Fig. 9(c)), and had developed due to stress redistribution in the sample after stage 57 (approx. 230 MPa). The size of the defect in zone 1 at 600 MPa is fairly large and creeps closer to the surface of the sample.

The analysis of damage is supported by knee-points of the stress–strain diagram that show the onset of macro damage and its development. The threshold for identification of damage does not depend on the absolute value of local major strains and is not affected by the interpolation of strains in a registered strain field. In thick laminates, damage in laminas below the surface layer does not reflect on the surface strain field. However, for qualitative damage analysis of thin composite laminates, the strain mapping technique has proven to be an effective tool. A common useful feature of this technique for analyzing strain is that local high strain areas relate to more compliant regions, such as local pre-existing defects or irregularities (e.g., epoxy pockets or fiber misalignments). Therefore, the combined results of an NDT test such as Flash Thermography and a monitoring technique (e.g., strain mapping) can lead to an understanding of the internal structure of the composite.

5. Adaptive algorithm for online damage detection

Data post processing is either performed in the harvesting part of the system or in post-mortem monitoring. This section presents the application of the strain mapping technique for adaptive online detection of damage initiation and development in a composite laminate. The procedure discussed in Section 4 is used with some modifications to assess the strain gradients simultaneously as the load applies to the structure in order to perform damage initiation and propagation, and strength prediction. As the sample deforms, the filtered strain tensor gets updated. Thus, at each stage of loading, time-wise filtering is used to obtain the filtered major strain. The linear-regression filtering method can be used in the

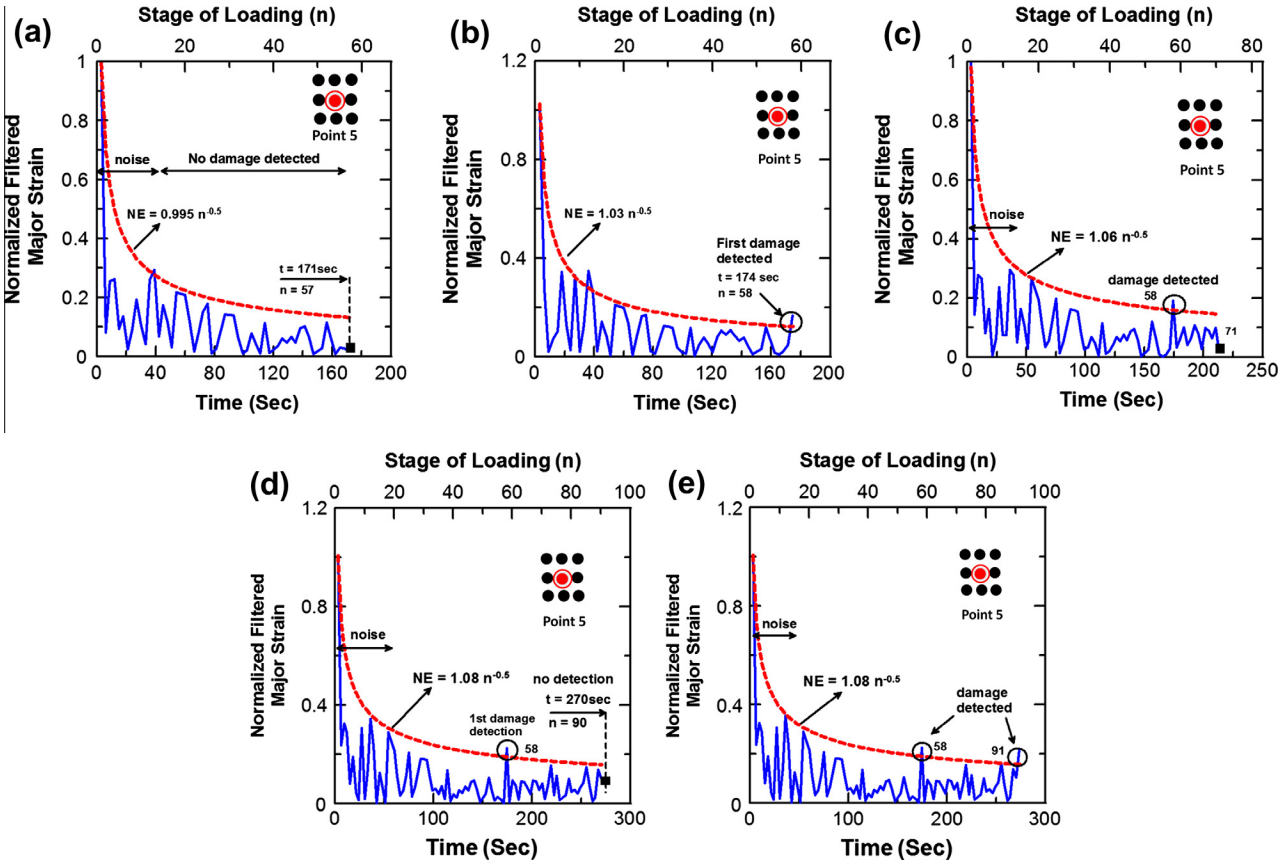

Fig. 10. Online damage detection at zone 1 using adaptive strain mapping technique.

elastic deformation regime [28]; however, the range of linear deformation is not known, and it can vary from sample to sample. For the sake of consistency, the same 4th order polynomial was used in this study. The threshold of damage identification was updated as the load was applied gradually to the specimen. The threshold function was introduced as $NE = c \times n^d$ and as evident from Fig. 10, "d" is constant as NE continually updates. The statistical readings were collected for all points of the token throughout the strain mapping area each time a load was applied. As the absolute amount of noise is almost constant, the relative noise level decreases while the load increases. The normalized filtered major strain exceeds the limits as a strain disturbance, such as when a sudden crack (e.g., at stage 58) occurs. While the crack exists at the location of the pre-existing defect, load re-distribution in the composite structure occurs (e.g., stages 58–90) as the applied load increases up to the next critical deformation level (e.g., stage 91).

6. Conclusions

The work presented here is an attempt to describe the link between NDT and monitoring techniques in the characterization of damage in composite structures. The results show the fundamental need for understanding the damage behavior of advanced composites and the success of NDT/monitoring systems to characterize the initiation and propagation of damage. Strain measurements obtained from the optical extensometer were used to plot the stress–strain diagram. Results show that although resolution of DIC is an issue to determine strain field, DIC is still a powerful technique in the determination of flaws (damage initiation and propagation) in composite materials, especially at more advanced stages of deformation where noise is less influential. Nonlinear time-regression analysis of the registered strain field was used to obtain a filtered strain tensor. The envelope of averaged relative noise levels was used as the damage initiation threshold. Combining Flash Thermography and strain mapping techniques proved to be successful in locating the damage initiation and development and for assessing the effects of pre-existing surface and subsurface defects on the macro-level mechanical behavior of thin composite materials. The proposed methods can be successfully applied for adaptive on-line detection of surface/subsurface damage in composite structures.

Acknowledgments

The research leading to these results has received funding from Pipe Reconstruction Inc., Phoenix, Arizona, under agreement No. 12-092212.

References

[1] Kumar S, Murthy Reddy KVVS, Kumar A, Rohini Devi G. Development and characterization of polymer ceramic continuous fiber reinforced functionally graded composites for aerospace application. Aero Sci and Tech, in press.
[2] Edgren F, Mattsson D, Asp LE, Varna J. Formation of damage and its effects on non-crimp fabric reinforced composites loaded in tension. Compos Sci Technol 2004;64(5):675–92.
[3] Mattsson D, Joffe R, Varna J. Damage in NCF composites under tension: effect of layer stacking sequence. Eng Fract Mech Fract Compos Mater 2008;75(9):66–82.
[4] Mikhaluk DS, Truong TC, Borovkov AI, Lomov SV, Verpoest I. Experimental observations and finite element modeling of damage initiation and evolution in carbon/epoxy non-crimp fabric composites. Eng Fract Mech Fract Compos Mater 2008;75(9):2751–66.
[5] Beaumont PWR, Dimant RA, Shercliff HR. Failure processes in composite materials: getting physical. J Mater Sci 2006;41:6526–46.

[6] Lomov SV, Ivanov DS, Truong TC, Verpoest I, Baudry F, Vanden Bosche K, et al. Experimental methodology of study of damage initiation and development in textile composites in uniaxial tensile test. Compos Sci Technol 2008;68:2340–9.
[7] Vallons K, Lomov SV, Verpoest I. Fatigue and post-fatigue behavior of carbon/eoxy non-crimp fabric composites. Composites: Part A 2009;40:251–9.
[8] Markatos DN, Tserpes KI, Rau E, Markus S, Ehrhart B, Pantelakis Sp. The effects of manufacturing-induced and in-service related bonding quality reduction on the mode-I fracture toughness of composite bonded joints for aeronautical use. Composites: Part B, doi.org/10.1016/j.compositesb.2012.05.052.
[9] Giordano M, Calabro A, Esposito C, D'Amore A, Nicolais L. An acoustic-emission characterization of the failure modes in polymer-composite materials. Compos Sci Technol 1998;58(12):1923–8.
[10] Wen J, Xia Z, Choy F. Damage detection of carbon fiber reinforced polymer composites via electrical resistance measurement. Composites Part: B 2011;42:77–86.
[11] Wang XJ, Chung DDL. Short carbon fiber reinforced epoxy coating as a piezoresistive strain sensor for cement mortar. Sens Actuat A 1998;71(3):208–12.
[12] Takeda S, Obabe Y, Takeda N. Delamination detection in CFRP laminates with embedded small diameter fiber bragg grating sensors. Composites Part: A 2002;33:971–80.
[13] Abry JC, Choi YK, Chateauminois A, Dalloz B, Giraud G, Salvia M. In situ monitoring of damage in CFRP laminates by means of AC and DC measurements. Compos Sci Technol 2001;61:855–64.
[14] Todoroki A. The effect of number of electrodes and diagnostic tool for monitoring the delamination of CFRP laminates by changes in electrical resistance. Compos Sci Technol 2001;61:1871–80.
[15] Lei SY, Young RJ. Deformation of PBO/epoxy plain weave fabric laminate followed using Raman spectroscopy. Compos Struct 2001;52:315–22.
[16] Masters JE, Ifju PG. A phenomonological study of triaxially braided textile composites loaded in tension. Compos Sci Technol 1996;56:347–58.
[17] Naik RA, Ifju PG, Masters JE. Effect of fiber architecture parameters on deformation fields and elastic moduli of 2D braided composite. J Compos Mater 1994;28:656–81.
[18] Truong Chi T, Vettori M, Lomov SV, Verpoest I. Carbon composites based on multi-axial multiply stitched performs, Part 4: mechanical properties of composites and damage observation. Composites: Part A 2005;36:1207–21.
[19] Potluri P, Young RJ, Rashed K, Manan A, Shyng YT. Meso-scale strain mapping in UD woven composites. Composites Part: A 2009;40:1838–45.
[20] Katerelos DG, McCartney LN, Galiotis C. Local strain re-distribution and stiffness degradation in cross-ply polymer composites under tension. Acta Mater 2005;53:3335–43.
[21] Hale RD, Villa M. Influence of opposing wave nesting in compression-loaded composites. J Compos Mater 2003;28(13):1149–66.
[22] Hale RD. An experimental investigation into strain distribution in 2D and 3D textile composites. Compos Sci Technol 2003;63:71–85.
[23] Ifju PG, Masters JE, Jackson WC. The use of moiré interferometry as an aid to standard test-method development for textile composite materials. Compos Sci Technol 1995;53:155–63.
[24] Lee JR, Molimard J, Vautrin A, Surrel Y. Digital phase-shifting grating shearography for experimental analysis of fabric composites under tension. Composites Part: A 2004;35:849–59.
[25] Yekani Fard M, Liu Y, Chattopadhyay A. Characterization of epoxy resin including strain rate effects using digital image correlation system. J Aerospace Eng 2012;25(2):308–20.
[26] Yekani Fard M, Liu Y, Chattopadhyay A. Analytical solution for flexural response of epoxy resin materials. J Aerospace Eng 2012;25(3):395–408.
[27] Yekani Fard M, Chattopadhyay A, Liu Y. Multi-linear stress–strain and closed-form moment curvature response of epoxy resin materials. Int J Mech Sci 2012;57(1):9–18.
[28] Lomov SV, Ivanov DS, Verpoest I, Zako M, Kurashiki T, Nakai H, et al. Full-field strain measurements for validation of meso-FE analysis of textile composites. Composites Part: A 2008;39:1218–31.
[29] Lomov SV, Ding X, Hirosawa S, Kondratiev SV, Molimard J, Nakai H. FE simulations of textile composites on unit cell level: validation with full-field strain measurements. In: Proceedings of the 26th SAMPE-Europe conference; 2005. p. 28–33.
[30] Ivanov D, Vandenbosche K, Ivanov S, Baudry F, Lomov S, Verpoest I. Strain mapping analysis of various textile composite and noise filtering of the data. In: Proceedings of the optimess-2007 workshop, Leuven, 28–30 May; 2007.
[31] Nicoletto G, Anzelotti E, Riva E, Roncella R. Mesomechanic strain fields in woven composites: experiments vs. FEM modeling. In: Proceedings of the optimess-2007 workshop, Leuven, 28–30 May; 2007.
[32] Quek SC, Waas AM, Shahwan KW, Agaram V. Compressive response and failure of braided textile composite: Part 1 – experiments. Int J Non-linear Mech 2004;39:635–48.
[33] Godara A, Raabe D. Influence of fiber orientation on global mechanical behavior and meso-scale strain localization in a short glass–fiber reinforced epoxy polymer composite during tensile deformation investigated using digital image correlation. Compos Sci Technol 2007;67(11–12):2417–27.
[34] Canal LP, Gonzalez C, Molina-Aldareguia JM, Segurado J, Llorca J. Application of digital image correlation at the micro-scale in fiber-reinforced composites. Composites Part: A 2012;43(10):1630–8.
[35] Gao X, Shao W, Ji H. Study on mechanical properties and damage behaviors of Kevlar fiber reinforced epoxy composites by digital image correlation technique under optical microscope. SPIE 7657; 2010 doi:10.1117/12.866731.
[36] Sun JG, Deemer C, Ellingson WA. Thermal imaging measurement and correlation of thermal diffusivity in continuous fiber ceramic composites. In: Thermal conductivity Gaal PS, Apostlescu DE, (editor); 1999, vol. 24, p. 612–22.
[37] Maldague XPV. Introduction to NDT by active infrared thermography. Mater Eval 2002;6(9):1060–73.
[38] Shepard SM, Hou Y, Ahmed T, Lhota JR. Reference-free interpretation of flash thermography data. Insight Brit Inst NDT 2006;48(5).
[39] Greve L, Pickett AK. Modeling damage and failure in carbon/epoxy non-crimp fabric composites including effects of fabric pre-shear. Composites Part: A 2006;37(11):1983–2001.
[40] ASTM D3039/D 3039M-00 Standard test method for tensile properties of polymer matrix composite materials (reapproved 2006).
[41] ASTM E2582-07. Standard practice for infrared flash thermography of composite panels and repair patches used in aerospace applications.
[42] Daggumati S, De Baere I, Van Paepegem W, Degrieck J, Xu J, Lomov SV, et al. Local damage in a 5-harness satin weave composite under static tension: Part 1 – experimental analysis. Compos Sci Technol 2010;70:1926–33.
[43] Tang X, Whitcomb JD. Progressive failure behavior of 2D woven composites. J Compos Mater 2003;37(14):1239–59.
[44] John S, Herszberg I, Coman F. Longitudinal and transverse damage taxonomy in woven composite components. Composites Part: B 2001;32:659–68.
[45] Sugimoto K, Nakai A, Hamada H. Effect of lamination sequence on mechanical behavior of woven composites. In: Proceedings of the 7th international conference on textile composites (TexComp-7); 2004. p. 1–4 [Textile 22].